Estudios en honor de
Francisco Javier Domínguez
AUCh, 5ª Serie, Nº 8 (1985): 139-175

WING TIP VORTEX ROLL-UP: AN EXPERIMENTAL AND THEORETICAL CHALLENGE

José Carlos Quadrelli and Cesar Farell
Universidad de Minessotta

I. Introduction

The study of vortex flows is of critical significance and interest to the hydrodynamician, both because of the varied and direct applications to numerous engineering problems (to name a few: intake flows; tornadoes; wing and propeller theory; vortex shedding from bluff bodies; three-dimensional (horseshoe) vortices around bridge piers of other cylindrical structures or buildings, immersed in boundary layers; other vortices associated with boundary layer flows of various kinds), and because of the attractive and intriguing nature of the flow patterns that result. These flows are characterized generally by their extreme unsteadiness which, coupled with a strong sensitivity to external disturbances, poses a challenge as yet not fully resolved for experimental measurements and theoretical analyses. As a result, available data and theory are inadequate in most instances.

Given the contributions of Prof. Domínguez to hydraulic engineering education and research, basic and applied, the topic of vortex flows seems rather appropriate for this work. Specifically, the problem of tip vortex roll-up for an elliptically-loaded wing will be examined, reviewing available theories and experimental data, with particular reference to measurements recently carried out at the St. Anthony Falls Hydraulic Laboratory and reported in detail in Quadrelli [23]. The emphasis herein will be on the review of this most fascinating phenomenon.

Wing-tip vortices are characterized by relative spatial stationarity, which allows for the formulation of simplified flow models and, perhaps even more importantly, permits the measurement of vortex core velocities utilizing the non-intrusive technique of Laser Doppler Velocimetry. Thus, this problem affords the possibility of improving our understanding of vortex flow dynamics, and has been chosen for this reason for the work reported herein and in the above-mentioned reference. For a general theory, the reader is referred to the treatises of Von Mises [19] or Milne-Thomson [18]. References to these two works will be freely made to make the presentation as concise as possible, but a review of the Rankine vortex and of Prandtl's tip vortex analysis is given for ease of reference and discussion.

Historically, studies of the tip-vortex roll-up process which characterizes the flow around all finite three-dimensional lifting surfaces can bee traced back to the beginning of this century. Many attempts, theoretical and experimental, have been made to explain the mechanics of the process but, although several useful models have been put forth, a complete understanding of the problem is yet to be achieved. The roll-up can be explain, qualitatively, either as a crossflow due to the pressure difference between the two sides of the lifting surface or, alternately, in terms of the vortex sheet that must be obtained of necessity behind any such surface. The vortex sheet, composed of an infinite number of vortex lines, is shed from the lifting surface, and it is the sum of the contributions of the velocity fields induced by these lines that leads to the roll-up and to the appearance of the tip vortices.

The known tip-vortex models can be classified chronologically into four generations [28] to give an overall view of their historical development:

1) semi-two dimensional inviscid theory (Prandtl [7, 18]; Betz [5]; 1920's and 30's);
2) Rankine model combined with experimental results (McCormick [17]; 1950's and 60's);
3) viscous models with axial core flows (Batchelor [4]; Moore and Saffman [20]; 1960's and 70's);
4) models based on numerical studies (1980's ?).

II. The Rankine vortex

The solution of the Navier-Stokes and continuity equations for steady, incompressible circular flow having only a tangential velocity component (v_θ) is of the following form:

$$v_\theta = C_1 r + C_2/r$$

where C_1 and C_2 are arbitrary constants. The Rankine vortex model divides the flow into two regions, in each of which one of the above constants is zero. In the inner region $C_2 = 0$ and a forced or rotational vortex is present. The rotation there is equivalent to that of a rigid body. This region extends from $r = 0$ to $r = r_c$ where r_c is the radius of the rotational core. Beyond that, $C_1 = 0$ which represents a free or irrotational vortex.

Let us determine the expressions for the velocities and pressures in these regions by first considering a vertical-axis free-surface vortex.

For the forced vortex, the tangential velocity is given by:

$$v_\theta = \Omega r \tag{II.1}$$

where Ω is the angular velocity of the vortex, a constant for rigid-body rotation. One can relate Ω to the circulation of the vortex by applying the definition of circulation at the coreradius:

$$\Gamma = \int_0^{2\Pi} v_\theta r_c d\theta = \int_0^{2\Pi} \Omega_{r_c}^2 \, d\theta = 2\Omega\Pi r_c^2 \tag{II.2}$$

We have then

$$\Omega = \frac{r}{2\Pi r_c^2} \text{ and } v_\theta = \frac{\Gamma r}{2\Pi r_c^2} \tag{II.3}$$

The forced-vortex water-depth differential can be obtained by applying Euler's equation (or Bernoulli's equation modified through addition of the potential of the centrifugal forces) which gives:

$$h - h_c = \frac{\Omega^2 r^2}{2g} \tag{II.4}$$

where h_c is the water depth at the center of the vortex. If we evaluate this expression at the coreradius, using (II.3) for Ω:

$$h_r = h_c + \frac{\Gamma^2}{8\Pi^2 g r_c^2} \tag{II.5}$$

For the free vortex we have instead, using (II.2):

$$v_\theta = \frac{C_2}{r} = \frac{\Gamma}{2\Pi r} \tag{II.6}$$

and from Bernoulli's equation, evaluated at the coreradius, we get:

$$hr = h_0 - \frac{\Gamma^2}{8\Pi^2 g r_c^2} \tag{II.7}$$

where h_0 is the water depth at infinity. Equating (II.5) and (II.7), we get an expression for $h_0 - h_c$:

$$h_0 - h_c = \frac{\Gamma^2}{4\Pi^2 g r_c^2} \tag{II.8}$$

If a free surface is not present, h must be set equal to $z + p/\gamma$. For z = constant or for air flows, letting p_0 = pressure at infinity and p_c = pressure at the center of the vortex, one gets:

$$p_0 - p_c = \rho \left[\frac{\Gamma}{2\Pi r_c}\right]^2 \tag{II.9}$$

If the minimum pressure in the vortex core is equal to the vapor pressure (p_v), we can introduce the cavitation index:

$$\sigma = -Cp_{min} = \frac{p_0 - p_c}{\frac{1}{2}\rho U_0^2} \tag{II.10}$$

Thus, we can write:

$$\sigma = 2\left[\frac{\Gamma}{2\Pi U_0 r_c}\right]^2 \tag{II.11}$$

Note that Rankine's model does not permit the determination of the core radius by itself since the pressure at the vortex core is also unknown. Thus, it is used as a framework for other, more complete models.

III. Prandtl's model

The basic assumption of Prandtl's inviscid tip-vortex model is that the kinetic energy per unit length of the vortex system (consisting of the two vortices rolled up on each side of the wing) equals the induced drag of the wing [7, 17, 18]. In the other words, it is assumed that the work done in moving the wing against the induced drag is used entirely to increase the kinetic energy of the vortices being shed. In reeality, this work is partially dissipated due to friction. Thus, Prandtl's model should overestimate the energy of the vortices. Actually, estimates of the vortex core radius

(defined as the radius where the maximum tangential velocity occurs) obtained using Prandtl's model are an order of magnitude larger than experimentally determined values [17, 23]. The magnitude of this discrepancy sheds doubts on the validity of a completelly rolled-up vortex sheet as representative of the actual vortex system. The measurements show that the vortex core circulation (calculated at the radius of maximum tangential velocity) is much less than the circulation at the wing midspan, as assumed in Prandtl's calculations (see below). Furthermore, the velocity distribution outside the radius of maximum tangential velocity does not exhibit the 1/r dependence of the model, except possibly at downstream distances an order of magnitude larger than the wing chordlength. Pradtl's model is still of interest, however, as a starting point for an analysis of the flow, and a concise review of it is given in this section.

Prandtl adopted the Rankine vortex for his calculations. Thus, the kinetic energy of the vortices can be divided into two components, one being the energy of the cores (Kc), and the other, the energy of the outer or irrotational flow (Ko). Thus, we have:

$$Ki = Kc + Ko = Di \tag{III.1}$$

where Di is the induced drag and Ki the total kinetic energy per unit length of the vortices.

The flow is studied in a plane, perpendicular to the free-stream direction and downstream of the wing, which has become known as the Trefftz Plane (see Fig. III.1). Neglecting the velocity components normal to this plane, and using (II.3) for the tangential velocity, the kinetic energy per unit length in the two vortex cores is given simply by the following integral taken around both cores:

$$Kc = 2 \cdot \frac{1}{2} \rho \int\int_S v_\theta^2 \, dS = \rho \int_0^{r_c} \int_0^{2\Pi} v_\theta^2 r d\theta dr = \frac{p\Gamma^2}{8\Pi} \tag{III.2}$$

To calculate the kinetic energy of the irrotational flow, one can use a line-integral form in terms of the stream function ψ [18, pg. 78; also 4, pg. 529):

$$K_0 = \frac{1}{2} \rho \int_c \psi \vec{u} \bullet d\vec{r} \tag{III.3}$$

The vectors are defined by: $\vec{u} = u\vec{i} + v\vec{j}$ and $d\vec{r} = dx\vec{i} + dy\vec{j}$. For the two-vortex system, the integration is performed around a curve that

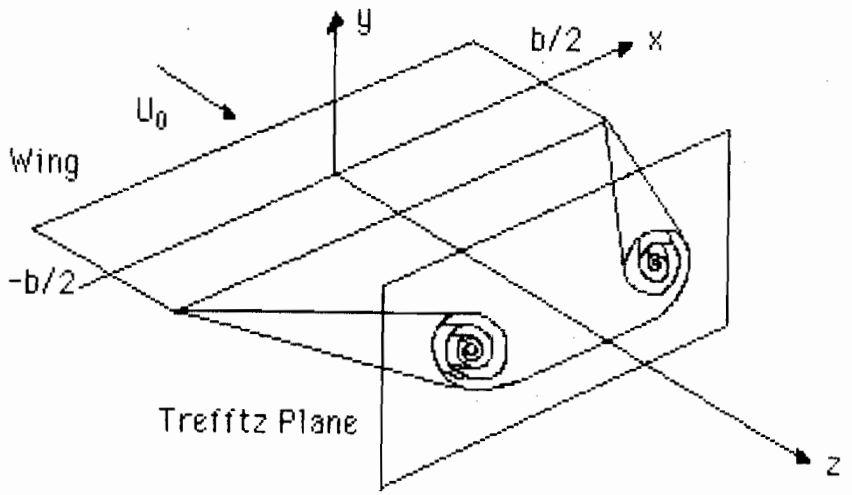

Fig. III.1. The Trefftz plane.

encompasses the two vortices (which are removed from the region of integration by means of a cut). The integral around the external circle goes to zero as $r \to \infty$. On the boundaries of the vortex cores, one has

$$r = r_c,\ \psi = \psi_c,\ v_\theta = \Gamma/2\Pi r_c$$

and therefore, we end up with:

$$Ko = 2 \cdot \frac{1}{2} \rho\, \psi_c \int_c (\Gamma/2\Pi r_c) r_c d\theta = \rho \psi_c \Gamma \qquad \text{(III.4)}$$

To determine ψ_c, we must first determine the location of the vortex cores. The point vortices or vortex singularities are located at $\pm b'/2$. The distance b′ can be related to the wing span b as follows. The impulse of the pair of vortices for a length $U_0\Delta t$ is $\rho\Gamma b' U_0 \Delta t$ [18, pg. 209] and the lift force, which is the time derivative of the impulse, is then given by

$$L = \rho U_0 \Gamma_0 b' = L_0 b' \qquad \text{(III.5)}$$

where Γ_0 and L_0 are the circulation and the lift per unit length, respectively, and midspan. The overall and midspan sectional lift coefficients are defined by:

$$C_L = \frac{L}{\frac{1}{2}\rho U_0^2 S} \quad \text{(III.6)}; \qquad c_{l_0} = \frac{L_0}{\frac{1}{2}\rho U_0^2 c_0} \quad \text{(III.7)}$$

where S is the area of the wing (= bc_m, where c_m is the average chord) and C_0 is the midspan chord. Dividing (III.6) by (III.7) and using the relation between L and L_0, one gets:

$$\frac{b'}{b} = \frac{C_L}{c_{l_0}} \frac{c_m}{c_0} = \frac{C_L}{c_{l_0}} \frac{b}{c_0} \frac{1}{AR} \quad \text{(III.8)}$$

where $AR = b/c_m$ is the wing aspect ratio.

To determine the value of the stream function at the coreradius, it must be noticed that since the streamlines are displaced due to the mutual influence of both vortices, the cores' centers do not coincide with the locations of the point vortices. Let the complex potential be $\omega = \phi + i\psi$, where ϕ is the velocity potential. If we define the complex number $Z = x + iy$, the complex potential for the system of two vortices is given by:

$$\omega(Z) = -(i\Gamma/2\Pi)[\log(Z - b'/2) - \log(Z + b'/2)]$$

If we substitute $x + iy$ for Z in the last expression and take the imaginary part, we will get the equation for the stream function outside the cores:

$$\psi = \frac{\Gamma}{4\Pi} \ln \left[\frac{(x + b'/2)^2 + y^2}{(x - b'/2)^2 + y^2} \right] \quad \text{(III.9)}$$

For $\psi = \psi_c$, we can write: $\dfrac{(x + b'/2)^2 + y^2}{(x - b'/2)^2 + y^2} = \exp(4\Pi\psi_c/\Gamma) = k$ (const.)

We can rearrange this expression to end up with:

$$\left[x + \frac{b'}{2} \frac{(1 + k)}{(1 - k)} \right]^2 + y^2 = \frac{b'^2}{4} \left[\frac{(1+k)^2}{(1-k)^2} - 1 \right] \quad \text{(III.10)}$$

which is of the form $(x - x_0)^2 + (y - y_0)^2 = r_c^2$, the equation of a circle of radius r_c and centered at (x_0, y_0). In our case, we have $x_0 = \pm a/2$ and $y_0 = 0$ and, as one can see from (III.10), $r_c^2 = (a/2)^2 - (b'/2)^2$ so that we get: $a/2 =$

$\pm\sqrt{[(b'/2)^2 + r_c^2]}$. Using this expression, we can rewrite the equations of the circles so that we end up with:

$$(x \pm b'/2)^2 + y^2 = 2x\{\sqrt{[(b'/2)^2 + r_c^2]} \pm b'/2\} \qquad \text{(III.11)}$$

Substituting (III.11) into (III.9), we evaluate ψ_c, which can now be combined with (III.4) to yield Ko:

$$Ko = \frac{\rho\Gamma^2}{4\Pi} \ln\left[\frac{\sqrt{[(b'/2)^2 + r_c^2]} + b'/2}{\sqrt{[(b'/2)^2 + r_c^2]} - b'/2}\right] \qquad \text{(III.12)}$$

Combining (III.2) and (III.12), we get the total kinetic energy per unit length:

$$Ki = \frac{\rho\Gamma^2}{8\Pi}\left[1 + 2\ln\left[\frac{\sqrt{[(b'/2)^2 + r_c^2]} + b'/2}{\sqrt{[(b'/2)^2 + r_c^2]} - b'/2}\right]\right] \qquad \text{(III.13)}$$

We must now equate Ki to the induced drag, Di, given by

$$Di = \frac{1}{2}\rho U_0^2 C_{Di} S = \frac{1}{2}\rho U_0^2 C_{Di} b^2 (c_m/b) = \frac{1}{2}\rho U_0^2 C_{Di} b^2/AR$$

where C_{Di} is the induced drag coefficient. Noting that $c_{l_0} = 2\Gamma_0/U_0 c_0$ (obtained by substituting the equality $L_0 = \rho U_0 \Gamma_0$ into the definition for c_{l_0}) and using (III.8) to substitute for c_{l_0}, we get:

$$Di = 2\rho\Gamma_0^2 \frac{C_{Di}}{C_L^2} AR\left[\frac{b'}{b}\right]^2 \qquad \text{(III.14)}$$

Equating (III.13) and (III.14), one can obtain the sought-after expression for the core radius, but before this is done one must assume that the circulation of the vortices (Γ) is equal to the circulation at the wing's midspan (Γ_0). After some algebraic manipulation, we arrive at the following result, expressed in dimensionless form:

$$\frac{2r_c}{b} = \frac{b'}{b}\left[\left[\frac{\exp[(8\Pi ARC_{Di}/C_L^2)(b'/b)^2 - 1/2] + 1}{\exp[(8\Pi ARC_{Di}/C_L^2)(b'/b)^2 - 1/2] - 1}\right]^2 - 1\right]^{1/2} \qquad \text{(III.15)}$$

Once r_c is determined by the above equation, the velocity distribution can be obtained by using the expressions of section II.

We will now simplify the above result for the case of the elliptically-loaded wing. The wing used in the experiments reported in [23] was not only elliptically-loaded, but also elliptic in shape (without twist). One then has:

$$S = \Pi b c_0/4 = b c_m \Rightarrow c_m/c_0 = \Pi/4 \tag{III.16}$$

and from the definitions of the lift coefficients:

$$C_L/c_{l_0} = Lc_0/L_0S = 4L/\Pi b L_0 \tag{III.17}$$

To relate the midspan lift, L_0, to the total lift, L, of the wing, one can integrate the lift per unit length over the wing. To do this, one must assume the flow to be two-dimensional (no crossflow). Although this is not a very accurate assumption for low aspect ratio wings, reasonable results can still be obtained in this manner as indicated in [19, pg. 273]. For an elliptically-loaded wing with invariable profile and without twist, the section lift coefficient c_l is actually constant over the span, the lift per unit length being simply proportional to the section chord length, c (see e.g. [19]). We have then

$$L = 2\int_0^{b/2} c_l \frac{1}{2}\rho U_0^2 c\,dx = c_{l_0}\rho U_0^2 \int_0^{b/2} c\,dx$$

Substituting the chord $c = c_0\sqrt{[1 - (2x/b)^2]}$, and C_{l_0} by its definition, one gets:

$$L = L_0(\Pi b/4) \Rightarrow C_L = c_{l_0} \tag{III.18}$$

as could be predicted from the constancy of c_l over the wing span. From (III.8), using (III.16) and (III.18), we get:

$$b'/b = \Pi/4 \tag{III.19}$$

We also have for an elliptically-loaded wing (see e.g. [19, pp. 239-243]):

$$L = \Pi\rho U_0\Gamma_0 b/4 \tag{III.20}$$

$$Di = \Pi\rho\Gamma_0^2/8 \tag{III.21}$$

$$C_{Di}/C_L^2 = S/\Pi b^2 = 1/\Pi AR \tag{III.22}$$

If one substitutes (III.19) and (III.22) into (III.15), a numerical value for the dimensionless core radius is finally obtained:

$$2r_c/b = 0.1731 \Rightarrow r_c = 0.08655b \qquad \text{(III.23)}$$

In Fig. IV.2, we have plotted the velocity profile using the above expression for core radius so that a comparison with Betz's model can be made.

IV. The theory of Betz.

Betz's inviscid roll-up model, developed in 1932 [5], remained practically dormant until the early 1970's when several researchers (e.g.Rossow [26] and Jordan [13]) revived it and applied it to more general span loadings. Although Moore and Saffman [20] had already stated that the Betz model did not conserve energy, it was considered a useful method to predict the characteristics of the potential flow field which is of prime importance in the case of vortices trailing from aircraft wings.

To construct his model, Betz used three well-known conservation theorems of vortex motion. The parameters conserved, namely circulation, center of gravity of vorticity and second moment of vorticity, are called integral invariants. These invariants relate the vorticity in the vortex sheet (assumed to be composed of a continuous vortex distribution) to that in the ensuing tip vortices. Betz also assumed that the roll-up of one vortex is independent of the presence of other vortices, which is not rigorously true. This is equivalent to considering a semi-infinite vortex sheet.

Betz reasoned that the outer portion of the vortex sheet (near the tip of the wing) would roll up first forming the center of the tip vortex. Each additional segment of the sheet would wrap itself around the preceding one until the center of the wing was reached. The last piece of the sheet would correspond to the vortex's maximum radius. This is depicted in Fig. IV.1.

As can be seen in Fig. IV.1, the vorticity shed from $x = b/2$ to $x = x_1$ will correspond to the vorticity present in the vortex core from $r = 0$ to $r = r_1$. In other words, since circulation equals the flux of vorticity, we have:

$$\Gamma(x_1) = \Gamma_v(r_1) \qquad \text{(IV.1)}$$

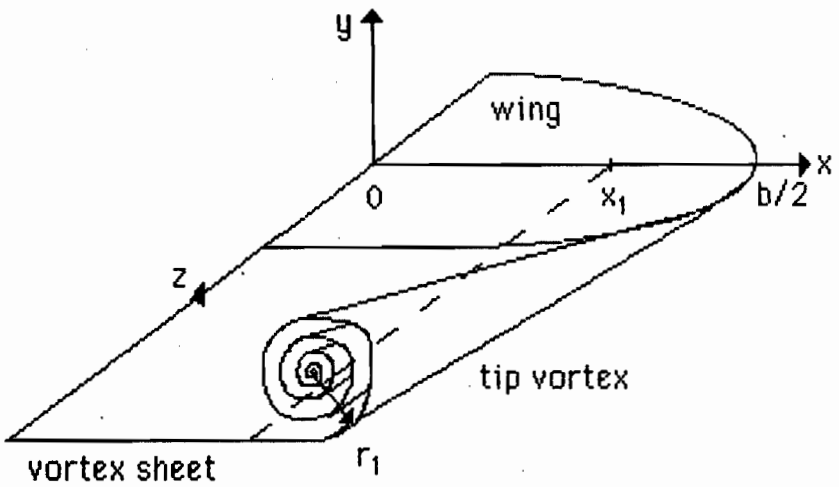

Fig. IV.1. Roll-up of vortex sheet

where Γ_v is the circulation of the tip vortex. This defines r_1 as a function of x_1: $r_1 = f(x_1)$. Thus, according to Betz, the circulation of the tip vortex is nowhere constant as it was in the irrotational region of Prandtl's model.

We will now determine the distribution of the circulation and the velocity field by assuming that the integral invariants of the vorticity distribution, as defined e.g. in [4, pp. 528-529], are also invariant when applied to the roll-up process depicted in Fig. IV.1. In addition to (IV.1), we have the following equations expressing the above-mentioned invariants:

$$x_c(x_1) = \frac{1}{\Gamma(x_1)} \int_{b/2}^{x_1} x \frac{d\Gamma(x)}{dx} dx \qquad \text{(IV.2)}$$

and

$$\int_{b/2}^{x_1} [x_c(x_1) - x]^2 \frac{d\Gamma(x)}{dx} dx = \int_0^{r_1} r^2 \frac{d\Gamma_v(r)}{dr} dr \qquad \text{(IV.3)}$$

where: $x_c(x_1)$ = abscissa of center of gravity of vorticity shed from wing tip to station x_1 (see Fig. IV.1).

Substituting $r = f(x)$ in the right-hand-side integral in (IV.3) and equating the integrands (possible because the roll-up is continuous and (IV.3) is valid for any x_1), we obtain:

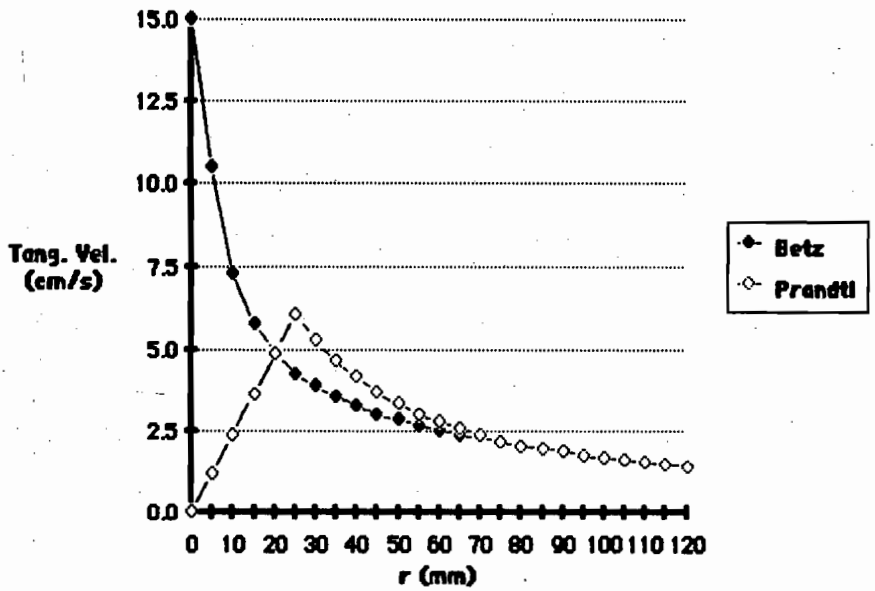

Fig. IV.2. Betz and Prandtl tangential velocity distributions for the foil used in the experiments at U_0 = 40 cm/s and α = 0°[23]

$$r_1 = |x_c(x_1) - x_1| \tag{IV.4}$$

For the case of elliptic loading, the circulation of the vortex sheet is given by:

$$\Gamma(x) = \Gamma_0\sqrt{[1 - (2x/b)^2]} \tag{IV.5}$$

Substituting this expression into (IV.4), one obtains the following expression for the vortex radius:

$$r_1 = \frac{b}{2}\,\frac{\Pi/4 - [\sin^{-1}(2x_1/b)]/2}{\sqrt{[1 - (2x_1/b)^2]}} - \frac{x_1}{2} \tag{IV.6}$$

Given r_1, x_1 must be obtained from the above expression, although this cannot be done directly. For $x_1 = 0$, which corresponds to a completely rolled-up vortex sheet, we can obtain the maximum radius from (IV.6):

$$r_{max} = \Pi b/8 \tag{IV.7}$$

Also, from (IV.2), the position of the center of gravity can be calculated:

$$x_c(0) = \Pi b/8 \qquad \text{(IV.8)}$$

Comparing the above two results, it appears that the two vortices will touch each other at midspan, a result inconsistent with the assumption of negligible interaction of the two vortices. The position of the center of gravity obtained here is the same as that given by Prandtl's model, equation (III.19).

In conclusion, to obtain the tangential velocity at a radius r_1, one must calculate x_1 from (IV.6), then $\Gamma(x_1)$ using (IV.5), and finally v_θ with (II.6). Since no rotational core has been considered, a singularity results at $r = 0$, where the velocity becomes infinite. In the potential flow region, the Betz method furnishes results close to those obtained by Prandtl as can be seen in Fig. IV.2 which indicates the results of a comparative calculation made for the particular foil used in the study reported in [23].

V. The viscous model of Moore and Saffman

In their 1973 paper, Moore and Saffman [20] advanced a viscous vortex model which they used as a basis for studying the axial flow in trailing vortices. They arrived at expressions for core radius, velocities and pressures by analytical means. We will summarize the basis concepts and results here and use them to derive equations for the core radius and maximun velocity dependent on Reynolds number and angle of attack.

To obtain initial conditions for the viscous vortex, the authors use a simplified inviscid model developed by Kaden (1931). In this method (see e.g. [7]) the wing is replaced by a semi-infinite lifting line with circulation $2\Gamma_0(x/b)^{1/2}$, where x is measured from the wing tip. This is justified on the grounds that in the initial stages of the roll-up, the two tip vortices do not interact significantly with each other.

The vortex sheet is then assumed to roll up into a tightly wound spiral whose turns are close enough together near the center, so that they can be considered concentric circles for calculation of the fluid velocity. The variation of the circulation with radius from the center is directly related to the corresponding variation of the circulation near the tip of the lifting line. From dimensional considerations one can then write:

$$\Gamma(r) = 2\gamma(\lambda r)^{1/2} \qquad \text{(V.1)}$$

where $\gamma=\Gamma_0/\sqrt{b}$ and λ is a so-called compression factor (dimensionless) which, for elliptic loading, the authors show it is equal to 1.5 if one uses Betz's assumption of conservation of angular momentum, and to 1.65 if conservation of energy during roll-up is assumed. Using (II.6) for v_θ, the authors derive an expression (already obtained by Kaden in a different manner) for the variation with time of the radial coordinate of one of the vortex lines that constitute the spiral. The resulting equation shows that the rolled-up portion of the spiral has a radius proportional to $(\gamma t)^{2/3}$, a result that, as the authors point out, follows directly on dimensional grounds regardless of the actual definition used for the rolled-up spiral radius.

Now, Moore and Saffman extend the above analysis to other loadings by substituting the exponent in (V.1) by 1-n, where n = 1/2 for elliptic loading. The radius of the spiral results proportional to $(\gamma t)^{1/(n+1)}$.

Using next the arguments that total head must be conserved between turns of the spiral, and that there must be a balance between radial pressure gradient and centrifugal force, estimates for pressure and axial velocity for $r \to 0$ are obtained, to be used in the viscous model as limiting conditions to match solutions.

Assuming that viscous effects are confined to an inner region of the flow, the viscous core, for which dimensional considerations indicate a radius of order $(\nu t)^{1/2}$, the authors use the boundary layer approximations to study the coreflow. The boundary conditions imposed are as follows:

1)$v_\theta = 0$ and v_z (axial velocity) is finite at r = 0;

2)v_θ, v_z and p should match the limiting form, for $r \to 0$, of the inviscid solution as r and the boundary-layer variable $r/(\nu t)^{1/2} \to \infty$;

3)v_θ and v_z are also given by the inviscid expressions for t = 0 (initial conditions).

The calculation is carried out neglecting the detailed spiral structure of the inviscid vortex and replacing it with a smoothed out velocity distribution, a valid procedure on account of viscous diffusion in the narrow spiral turns. Since the distance between turns in the inviscid vortex can be estimated from the equation of the spiral as being $2\Pi r^{n+2}/[(n+1)\gamma t]$, this is small compared to $(\nu t)^{1/2}$ if one has $r \ll (\gamma \nu^{1/2} t^{3/2})^{1/(n+2)}$.

The authors divide then the vortex into three regions:

I) a viscous core with radius $\approx (\nu t)^{1/2}$;

II) a tightly wound spiral region (distance between turns much less than the viscous core radius) with radius $\approx (\gamma \nu^{1/2} t^{3/2})^{1/(n+2)} > (\nu t)^{1/2}$;

III) an inviscid spiral with $r \approx (\gamma t)^{1/(n+1)}$.

Since region II effectively contains region I, the calculations would thus be valid for region I and a portion of region II very close to the viscous core.

The similarity variable $\eta = -r^2/4\nu t$ is used to solve the boundary-layer equations. The resulting tangential velocity distribution is differentiated with respect to radius to obtain the radius of maximum velocity, taken by most researchers as a measure of the vortex core radius (in an obvious analogy to the Rankine vortex). This is effectivelly the radius of region I as indicated above. For the case of elliptic loading, we arrive at:

$$r_c = 2.92(\nu t)^{1/2} = 2.92 c_0 (z/c_0)^{1/2} \mathbf{R}_0^{-1/2} \tag{V.2}$$

The last equality above was obtained by using $z = U_0 t$, which has been considered valid throughout this analysis. Notice that this result shows that the core radius grows downstream of the wing. If Betz' [5] assumption of conservation of angular momentum is used, one can show that the roll-up is complete and that the vortex no longer grows when $(\gamma t)^{2/3} \approx b/3$ (for elliptic loading). Note that for (V.2) to be valid r_c must remain much smaller than the radius of the inviscid spiral.

An expression for the maximum velocity can be obtained by substituting (V.2) into the velocity distribution. This results in:

$$v_{\theta_{max}} = \frac{0.384\, b^{0.5}\, U_0(\alpha - \alpha_0)}{(\nu z/U_0)^{0.25}(1 + 4b/kc_0)} \tag{V.3}$$

If we assume that after roll-up is completed, the vortex no longer grows, we can give an order-of-magnitude estimate of the time for this to occur (and the distance if we admit $z = U_0 t$) from the expression $(\gamma t)^{2/3} \approx b/3$. Substituting the expression for γ, we get:

$$t \approx (1/3)^{3/2} b^2/\Gamma_0 \tag{V.4}$$

and

$$z \approx (1/3)^{3/2} U_0 b^2/\Gamma_0 \tag{V.5}$$

Substituting (V.5) into (V.2) (assuming still that $r_c \ll b/3$, as can be easily checked) we get:

$$r_c \approx \frac{1.28b}{\mathbf{R}_0^{1/2}} \cdot \left[\frac{c_0 U_0}{\Gamma_0}\right]^{1/2} \tag{V.6}$$

We can now replace Γ_0 by its expression for elliptic loading [19] to get:

$$r_c \approx \frac{0.905}{R_0^{1/2}} \cdot \left[\frac{bc_0(1+\Pi AR/K)}{\alpha-\alpha_0} \right]^{1/2} \qquad (V.7)$$

It is interesting to note that the dimensionless coefficient Γ_0/c_0U_0 appears in the expression for r_c' equation (V.6). This parameter is one of the Π-numbers obtained in a dimensional analysis of the problem at hand (along with the Reynolds number) and it relates axial and tangential discharges (see also [10]).

The final expression (V.7) indicates that the core radius at complete roll-up is inversely proportional to the square root of the angle of attack. This is surprising since McCormick [17] arrived at an opposite result and the experiments also indicate that the core radius increases with angle of attack. We must bear in mind that such a comparison may not be completely valid since Moore and Saffman have not considered the effect to the velocity defect due to the boundary layer on the wing in the core radius calculation (although they later consider it when they calculate the axial velocity). This effect is implicit in McCormick's model which we will describe in the next section. Also, Moore and Saffman's model assumes laminar flow, and their results may not be valid except at small Reynolds numbers.

VI. The semi-empirical analysis of McCormick

In his 1962 paper, McCormick [17] presented what he called a semi-empirical analysis of the rolling-up of the vortex sheet. It is semi-empirical since the equations which are derived depend on certain constants that can be evaluated, as McCormick did, only experimentally. Although McCormick and other researches seem to have been able to obtain a good fit for their experimental points using his method, others have obtained contradictory results (e.g. [30]). Only time and more research can settle this controversy.

The most controversial of McCormick's assumptions is that the vortex core diameter is equal to the thickness of the boundary layer on the wing's pressure side. In other words, it will depend on the Reynolds number. With this assumption, it becomes necessary to establish where and how the boundary-layer thickness is calculated. McCormick assumed that the flow over the pressure side of the wing is diverted through a constant angle and leaves the wing at its tip (for the case of an elliptic wing). This can be visualized in Fig. VI.1.

The boundary-layer thickness is assumed to be given by:

$$\delta = k\ell/(R_\ell)^r \qquad (VI.1)$$

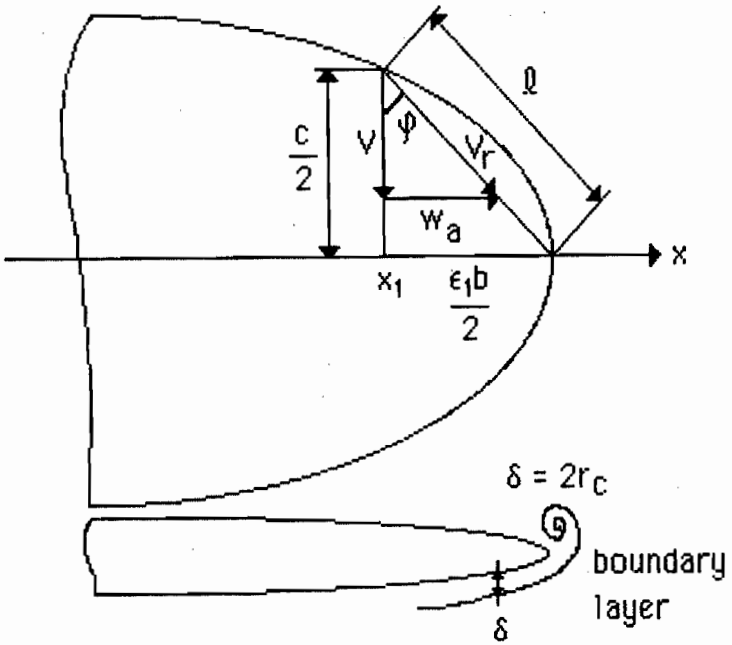

Fig. VI.1. Flow over lower (pressure) side of elliptic wing

where k and r are constants to be determined empirically and $\mathbf{R}_\ell = V_r\ell/\nu$ is the Reynolds number at the tip based on the relevant parameters. Introducing the wing span b and the Reynolds number $\mathbf{R}_0 = Vc_0/\nu$ based on maximum chord and on a reference velocity V (not necessarily the free-stream velocity), one obtains:

$$\frac{\delta}{b} = \frac{1}{\mathbf{R}_0^{\,r}}\left[\frac{k(\ell/b)}{\left[\frac{V_r}{V}\frac{\ell}{c_0}\right]^r}\right] \qquad \text{(VI.2)}$$

From Fig. VI.1. one has the following relations:

$$\ell = c/2\cos\varphi;\ V_r = V/\cos\varphi;\ \cos\varphi = 1/\sqrt{[1 + (w_a/V)^2]} \qquad \text{(VI.3)}$$

If we set $x/(b/2)=\xi$ (dimensionless), we can write (for an elliptic wing with invariable profile without twist) $c= c_0\sqrt{(1-\xi^2)}$ and $\Gamma = \Gamma_0\sqrt{(1-\xi^2)}$. Since we are very close to the wing tip, we can introduce the following approximation:

$$1 - \xi = \epsilon \Rightarrow 1 - \xi^2 = (1-\xi)(1+\xi) = \epsilon(2-\epsilon) \approx 2\epsilon$$

From the geometry (see Fig. VI.1) and substituting for c, one has: $\tan\varphi = \epsilon_1 b/c = \sqrt{(2\epsilon_1)}b/2c_0 \Rightarrow \sqrt{(2\epsilon_1)} = 2c_0\tan\varphi/b = 2C_0w_a/Vb$ where $\epsilon_1 = 1 - \xi_1$, $\xi_1 = x_1/(b/2)$. Now, the aspect ratio is given by: $AR = b/c_m = b^2/S = b^2/(\Pi bc_0/4) = 4b/\Pi c_0 \Rightarrow c_0/b = 4/\Pi AR$ Combining the above two results:

$$\sqrt{(1 - \xi^2)} = 2(4/\Pi AR)W_a/V \qquad \text{(VI.4)}$$

Using all of the above results, (VI.2) can be rewritten as

$$\frac{\delta}{b} = \frac{k}{R_0^{0.35}}\left[\frac{4}{\Pi AR}\right]^{1.65}\left[\frac{w_a}{V}\right]^{0.65}\left[1 + \left[\frac{w_a}{V}\right]^2\right]^{0.15} \qquad \text{(VI.5)}$$

In this equation, the value of r = 0.35, which McCormick obtained using his experimental results (as explained later), has been used.

We must now evaluate w_a/V. By using dimensional reasoning, McCormick proposed the following expression (reproduced here for the specific case of elliptic loading):

$$w_a/V = f(\Gamma/cV) \approx [K\Gamma/cV]^{n/2} = [K\Gamma_0/c_0V]^{n/2} \qquad \text{(VI.6)}$$

where K and n are constants to be experimentally determined (n/2 is used instead of n merely for convenience). It is interesting to observe that the above expression, as noted by Kuiper [14], produces rather large values for w_a (an order of magnitude larger than V as sample calculations show).

We now introduce the asumption $\delta = 2r_c$ and make use of the relations

$$c_{l_0} = 2\Gamma_0/c_0V \qquad , \qquad C_L = \alpha' dC_L/d\alpha',$$

(where $\alpha' = \alpha - \alpha_0$ = effective angle of attack). Using the values obtained experimentally by McCormick for k, K and n:

$$k = 0.31,\ K = 53.7,\ n = 1.6$$

we get finally an expression for the core radius (note that the angle of attack should be taken in radians):

$$r_c = \frac{0.155}{R_0^{0.35}}\left[\frac{4}{\Pi AR}\right]^{1.65}\left[26.85\alpha'\frac{dC_L}{d\alpha'}\right]^{0.52}\left[1 + \left[26.85\alpha'\frac{dC_L}{d\alpha'}\right]^{1.6}\right]^{0.15} \qquad \text{(VI.7)}$$

The exponent r was obtained in the following manner. First, curves of σ (cavitation number) versus Reynolds number were obtained experimentally. Then, the assumption $\sigma = -C_{P_{min}}$ ($C_{P_{min}}$ = minimun pressure coefficient) was made. Now, $C_{P_{min}}$ can be related to the tangential velocity at the edge of the vortex core (w_0) by first writing a Bernoulli equation between a point in the free stream and a point on the edge of the vortex core where it is assumed that $q^2 = U_0^2 + w_0^2$, that is, that any perturbation to the free-stream velocity in much smaller than w_0 itself. Denoting by P_r the pressure at that point, this result in:

$$P_r - P_0 = -\rho w_0^2/2 \tag{VI.8}$$

To relate P_r to the pressure at the center of the core (P_c), the Euler equation can be used to yield:

$$P_r = P_c + \rho w_0^2/2 \tag{VI.9}$$

If we combine (VI.8) and (VI.9) and divide the expression for $P_c - P_0$ by $\rho U_0^2/2$, we finally get:

$$\sigma = -C_{P_{min}} = (P_0 - P_c)/\frac{1}{2}\rho U_0^2 = 2(W_0/U_0)^2 \tag{VI.10}$$

In the above derivation a Rankine vortex model has been used, which is questionable since the calculation is applied in a region very close to the wing tip.

At this point, w_0 can be related to ξ_0, which is the non-dimensional abscissa of the edge of the vortex core, by using the Biot-Savart law for calculation of the induced velocity (actually upwash):

$$w_0 = w(\xi_0) = \int_{-1}^{1} \frac{d\Gamma/d\xi}{2\Pi(\xi_0 - \xi)}\, d\xi \tag{VI.11}$$

For the elliptically-loaded wing, this result in:

$$w_0 = \frac{\Gamma_0}{b}\left[\frac{\xi_0}{\sqrt{(\xi_0^2 - 1)}} - 1\right] \tag{VI.12}$$

Once w_0 is written in terms of ξ_0, σ can be plotted against ξ_0 and since $\xi_0 = 1 + \delta/b$ (considering that the center of the vortex core is located right

above the wing tip), one can obtain the variation of δ/b with R_0, and the exponent r.

VII. The complexities and pitfalls of experimental measurements of vortex-core velocities and dimensions

VII.1 *Laser Doppler Velocimetry*

Laser doppler velocimetry or anemometry (LDV or LDA) is one of the most effective methods for making velocity measurements in fluids. Its principal advantage is that it is a non-intrusive technique. In other words, it does not introduce any flow-altering obstruction into the fluid. This is of particular importance in vortex flow studies, not only because the scale of the phenomena of interest is generally small, but also because these flows are characterized by a strong sensivity to external disturbances.

The method consists in splitting into two the beam emitted from a laser and then focusing these two beams into a small ellipsoidal region called the probe volume. The light scattered from a particle that moves with the fluid and crosses this volume is picked up by a photo-detector. This instrument senses the doppler-shifted frequency difference between the two beams which strike the particle. The doppler shift exists due to the difference in the direction of the two beams.

Another way of understanding this is to consider the so-called fringe model. This model takes into account the fact that the two beams mutually interfere with each other and create a pattern of alternate light and dark fringes in the probe volume (see Fig. VII.1). When a particle crosses these fringes, it is alternately illuminated and obscured, thus emitting a series of light pulses whose frequency the photo-detector picks up. As can be inferred, this frequency shall be directly proportional to the velocity of the particle. The size of the probe volume is determined by the optics and the wavelength of the laser light.

To decrease the size of the probe volume (and thus increase the resolution), a beam expander can be placed between the beam splitter and the focusing lens. This component increases the diameter of the beams, so that after being focused by the lens, their diameter at the crossing point is actually reduced as equation (VII.1) below shows.

The dimensions of the probe volume must be determined to define the resolution of the LDV system. Initially, one must determine the diameter of the beams at their intersection. Since these beams have a Gaussian intensity distribution, their diameters are defined by means of the follo-

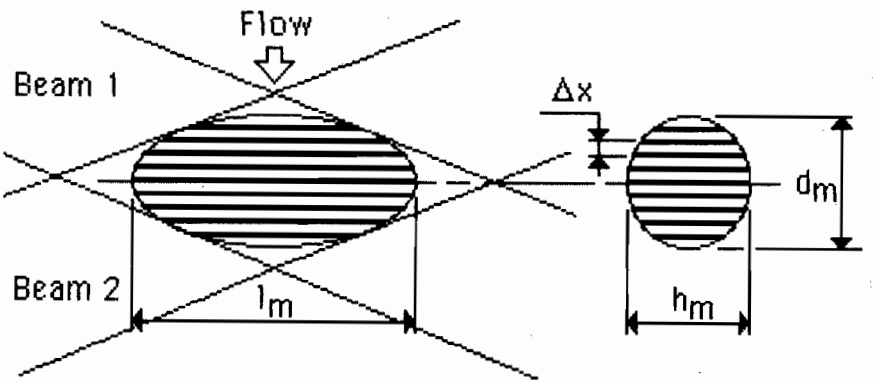

Fig. VII.1 Probe volume and fringe pattern

wing convention: the diameter extends out to the region where the intensity has dropped to e^{-2} of the maximum ($\approx$13.5%). One must also consider the refraction due to the glass window and the effect of the beam expander, which increases the beam diameter. Taking all this into account, one ends up with the following expression for the beam diameter at the crossing point (focus of lens) [2,25]:

$$d_e{-}2 = 4f'\lambda_3/\Pi(D_e - 2)\,E \qquad \text{(VII.1)}$$

and:

$$f' = I + d_g + Y' = f + (Y' - Y) \qquad \text{(VII.2)}$$

where (see Fig. VII.2):

$D_{e^{-2}}$ = diameter of the beam at exit from laser;
E = beam expander expansion ratio;
λ_3 = wavelength of laser light in water;
f' = combined focal length after refraction;
f = lens focal length.

To determine f', one must first calculate the angles κ_1, κ_2 and κ_3 as indicated in Fig. VII.2. This is simple since we know the focal length of the lens (f) and the beam spacing (d), both furnished by the lens manufacturer, and Snell's law of refraction. Note that κ_2 is the angle between the

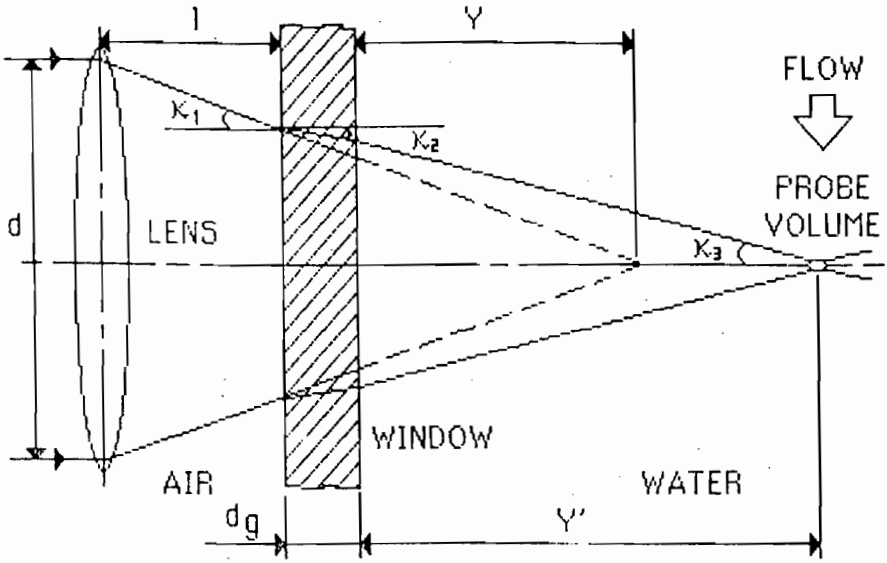

Fig. VII.2 Refraction of laser beams due to glass window.

incoming ray and the refracted ray in the glass. Thus, the following formulas apply:

$$\tan\kappa_1 = d/2f \qquad \text{(VII.3)}$$

$$m_1 \sin\kappa_1 = m_2 \sin\kappa_2 = m_3 \sin\kappa_3 \qquad \text{(VII.4)}$$

where m_1, m_2 and m_3 are the refractive indices of air, glass and water, respectivelly. The combined focal length f' is given by the following equation, which follows from (VII.2):

$$f' = f\frac{\tan\kappa_1}{\tan\kappa_3} + d_g\left[1 - \frac{\tan\kappa_2}{\tan\kappa_3}\right] + (l - d_g)\left[1 - \frac{\tan\kappa_1}{\tan\kappa_3}\right] \qquad \text{(VII.5)}$$

We now have all the necessary elements to calculate $d_{e^{-2}}$ and the dimensions of the probe volume. Also note that, since $f' = l + d_g + Y'$, the position of the probe volume (given by Y') can also be obtained. The length, width and height of the ellipsoidal probe volume are given, respectively, by [2,25]:

$$I_m = (d_{e^{-2}})/\sin\kappa_3 \qquad \text{(VII.6)}$$

$$d_m = (d_{e^{-2}})/\cos\kappa_3 \quad \text{(VII.7)}$$

$$h_m = d_{e^{-2}} \quad \text{(VII.8)}$$

The length of the probe volume is the most important for measurement of vortex-core velocities and dimensions, to ensure the necessary resolution. As one can see, I_m can be greatly decreased if a beam expander and a lens with small focal length are used. This was necessary for the study reported in [23]. By using a beam expander and a 120 mm focusing lens, the length of the probe volume was reduced from $I_m = 8.7$ mm (with a 350.6 mm lens) to $I_m = 0.46$ mm, while the width (and length) propped from $d_m = 0.47$ mm to $d_m = 0.07$ mm. The vortex core radius in that particular study had been estimated to be of the order of a few millimeters.

VII.2 *Vortex-core Measurements*

The emphasis in this section is on measurement techniques and errors. Velocity measurements reported and discussed fully in [23] are used as examples. These measurements were carried out in a 30.5 cm wide water channel at the St. Anthony Falls Hydraulic Laboratory. The model used was an elliptic planform foil with an aspect ratio of 3 and a NACA 66_2-415 (a=0.8) cross section. The half span of the foil was 152.4 mm and the average chord length 50.8 mm. The foil was mounted vertically, with the tip down, flush on a plexiglass plate placed 37.5 cm above the channel floor.

The single component LDV system used (TSI 9100-2 laboratory system) did not have a Bragg cell [2, 8] for frequency shifting, so that velocity directions could not be determined, only magnitudes. The system allowed for the measurement of axial and tangential velocity components (respectively in the flow direction, z, and in the spanwise direction, x; see Figs. III.1 and IV.1) and a component at 45° to the last two. Since velocity directions could not be detected, it was not possible to obtain the velocity distribution near the vortex core center (where the tangential velocity becomes zero and changes sign) by measuring only the tangential velocity component. On the other hand, if one measures the axial velocity and the 45-degree component, the tangential component can be computed from these two.

Two different methods were then used to obtain the tangential velocity profiles. In the first one, the tangential velocity was measured directly by aligning the probe volume fringes with the free-stream velocity. This procedure was satisfactory when the tangential velocities were relatively

large (larger than about 10 cm/s) since one must guarantee a minimum number of particles crossing the probe volume over a certain time interval, for the LDV system to respond. The second method consisted of measuring the axial velocity (v_z) and a component inclined at 45° to the free stream (v_{45}), and obtaining then the tangential velocity (v_θ) by decomposition of these two according to the following expression:

$$v_\theta = |v_z - v_{45}\sqrt{2}| \qquad \text{(VII.9)}$$

Since the axial velocity was always greater than the tangential component, a stronger signal could almost always be obtained in this manner.

A comparison of these two methods is presented in Figs. VII.3 and VII.4, which show tangential velocity plots measured for a foil angle of attack of 15° and a Reynolds number $R_0 = 47000$, in a plane perpendicular to the flow direction at z=203.2 mm (2 average chord lengths). All velocity plots begin at y=0 mm. This value is not measured in the coordinate system of the foil, but is simply the point where the traverse of the vortex core was begun, a procedure adopted because the exact location of the vortex core in relation to the foil is difficult to determine. Also note that all velocities are shown in absolute value. Curvesd have been drawn in the plots to permit an estimate of the core radius to be made. Since they were manually drawn they are subject to some subjective error. As an example, for some of the measured distributions in [23], a difference of about 15% was observed between curves drawn by different observers. The error is smaller when tangential velocities are measured directly.

In the range of foil angles of attack from 10 to approximately 15°, the vortex core could be located visually since minute air bubbles were entrained into that region. At lower angles of attack and closer to the foil, this visualization was not possible since not enough bubbles were present in the core. In these cases, dye was injected into the flow to obtain a rough estimate of the position of the vortex core, to serve as a reference point for the measurements. In general, the location of the center could be established fairly well once a traverse was completed, despite a small amount of vortex wandering.

The profiles in Figs. VII.3 and VII.4 illustrate the major advantages and drawbacks of each of the above-mentioned techniques for tangential velocity measurements. As expected, the direct tangential velocity measurement (herein referred to as M1) does not furnish accurate results near the center of the vortex core. Since the direction of the velocity vector cannot be sensed by the detector, all particle velocities which to into the

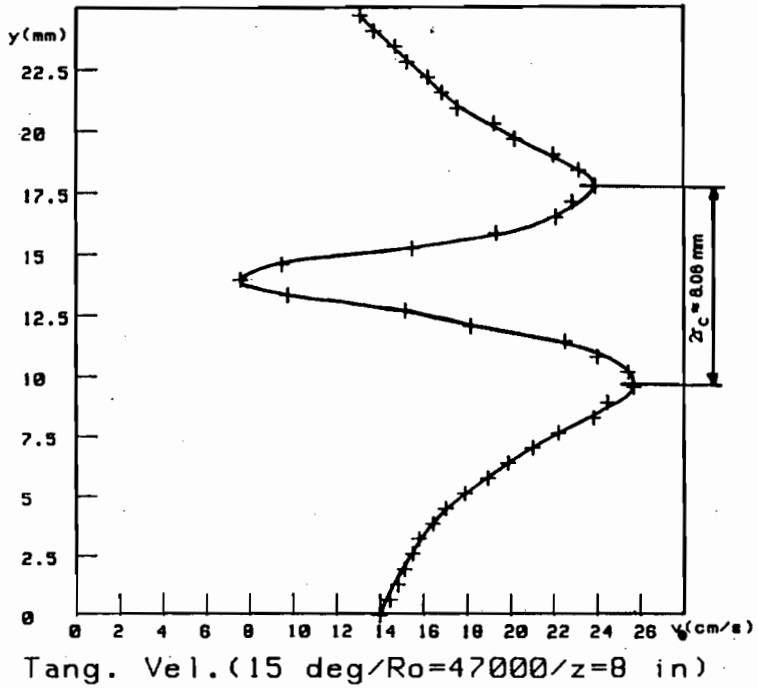

Fig. VII.3 Tangential velocity using measurement technique M1.

LDV average are computed as being positive, and a larger value is obtained (different from zero, in particular, at the center). This problem is eliminated in the second method (M2) since the decomposition permits the determination of the sign of the velocity vector. Thus, velocities very close to zero are measured. On the other hand, the scatter of the results is much greater in M2. Although a mean curve was drawn for that case so that an estimate of the core radius could be obtained, the error involved in such an estimate is much larger than for M1. The greater scatter in the results is most likely due to the fact that the velocity is obtained from two measurements so that the errors of the two are compounded. This can be analyzed as follows.

The standard deviations of the velocities (computed at each point) are roughly of the same order of magnitude for both the axial and the 45°-component measurements (approximately 5 to 10% of the mean value). Thus, from (VII.9) we can write (considering $\sigma_z \approx \sigma_{45}$):

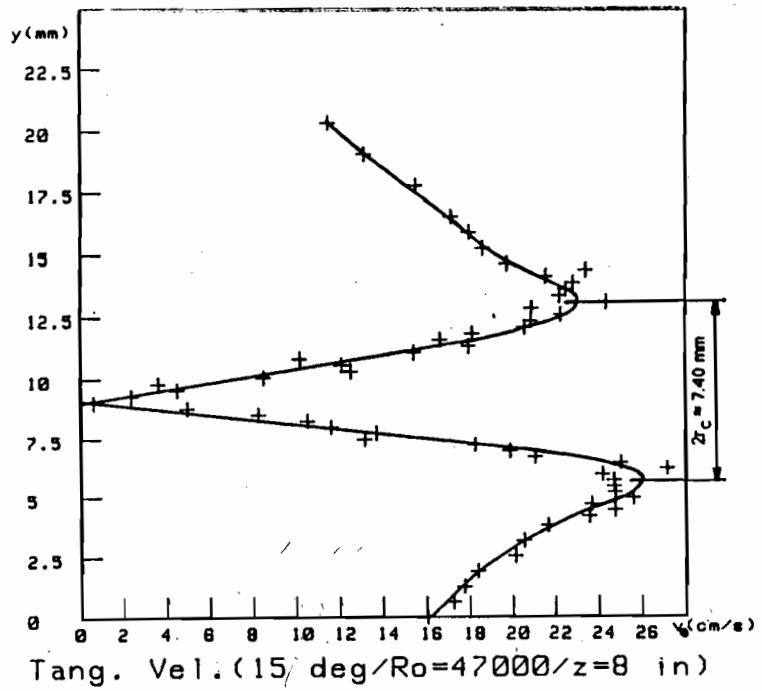

Fig. VII.4. Tangential velocity using measurement technique M2.

$$\sigma_\theta^2 = \sigma_z^2 + 2\sigma_{45}^2 \approx 3\sigma z^2 \Rightarrow \sigma_\theta \approx \sigma_z\sqrt{3} \qquad \text{(VII.10)}$$

Taking (VII.10) into account, the large oscillations near the maximum velocities in Fig. VII.4 can be explained. In the case, $\sigma_z \approx 1.4$ cm/s so that $\sigma_\theta \approx 2.4$ cm/s, which agrees roughly with the observed differences in that figure between adjacent points near the maximum velocity. Figure VII.5, which is the axial velocity plot corresponding to Fig. VII.4, shows much less scatter as was to be expected, since the axial velocity is measured directly.

The conclusion obtained from the above comparison is that the best practice is to combine the two techniques in the same measurement, using M1 in the regions of higher velocity and M2 inside the core region. The core radius can be estimated with less error with this method, and the location of the center of the vortex is also accurately obtained. A distance of 0.25 mm between points was used in [23] near the velocity peaks, with

0.5 mm being adopted elsewhere. Outside the core region, only a few points were needed to define the shape of the profile.

It is important to note that this strategy is only applicable if the tangential velocities exceed a certain minimum value, on the order of 9 to 10 cm/s here. As mentioned before, lower speeds were difficult to track using M1. This presented a problem at lower angles of attack and/or Reynolds numbers, where M2 had to be used over most of the traverse.

VII.3 *Additional Considerations*

Vortex wandering was observed in both the vertical and horizontal planes, casting some doubt as to the repeatability and validity of the velocity measurements. An attempt was made to estimate the magnitude of the oscilations by observing the position of the core (when it was made visible by naturally entrained air bubbles) with respect to the beam crossing point. A rough estimate of ± 1.27 mm for both planes was obtained at maximum discharge and $\alpha = 15°$. Baker et al [3] accounted for vortex wandering by supposing it was due mainly to free-stream turbulence. They estimated an eddy diffusivity from pictures of vortices marked with dye and incorporated it into a probability density function. This procedure permitted them to obtain better agreement with their experimental results. This was not attempted for the experiment reported in [23] since the rather involved calculations did not appear necessary in light of the results obtained.

The repeatability of the measurements was checked with the following two techniques. First, a back-and-forth selection of measurement locations was used so that a check of the precision and hystheresis of the positioning equipment and the stationarity of the flow could be made. This was used to acquire the data in Fig. VII.4. The positioning error was estimated to be of the order of 0.05 mm. As one can see from the figure, this error does not affect substantially the definition of the velocity profile.

The second experiment undertaken to check repeatability was to make one traverse of the vortex core and repeat it immediately afterwards in the opposite direction. As Fig. VII.6 shows, the overlapping of points was reasonably good, most of them falling on the same curve. Somewhat larger errors are present in the core, where the variation of the velocity is larger. This is most likely due to positioning error, but again it has no serious effect on the velocity profile.

Another question which arose was whether one could traverse the vortex in the plane of its axis. To investigate this, measurements were

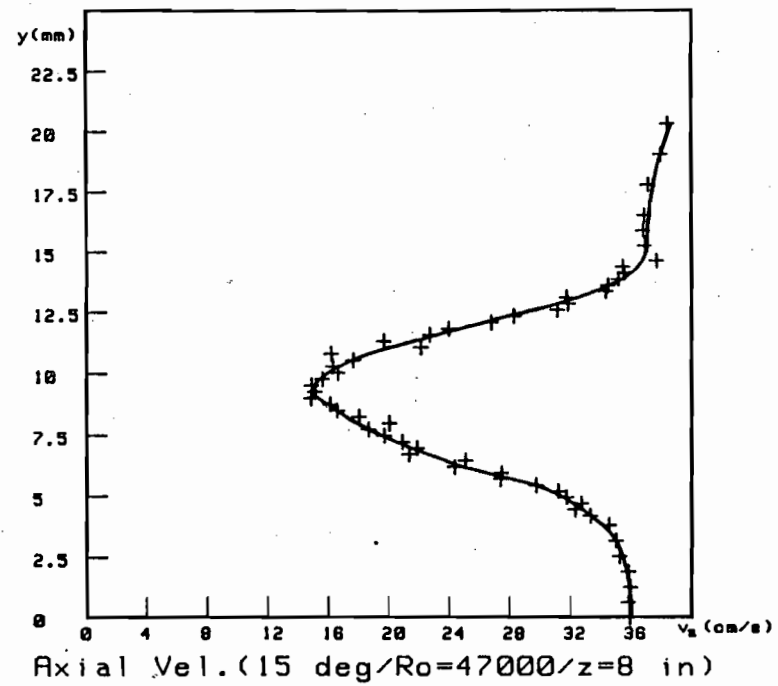

Fig. VII.5 Axial velocity distribution corresponding to Fig. VII.4.

carried out at 3 heights, first in a plane containing the assumed (as visualized) position of the axis, and then in planes 2.5 mm above and below it. As expected, the central traverse produced the largest velocity peaks, but it also appeared to have the smallest core radius of the three. This has to do with the structure of the vortex core, which is evidently not circular, and has obvious implications in regard to the definition of the core "radius". The measured velocity distributions were not only assymetric as Figs. VII.3 and VII.4 show, but the overall shape of the vortex core appeared to be possibly some kind of a Cassini oval. For further analysis of this point, reference is made to [23].

The core radii were estimated by taking one half of the distance between tangential velocity peaks. The scatter in the values of the radii shown in Figs. VII.3, VII.4 and VII.6 is typical of the results and highlights the complexities of the flow and of the measurements themselves. In view of the discussion above, these radii might perhaps be more properly referred to as typical coreradial length scales.

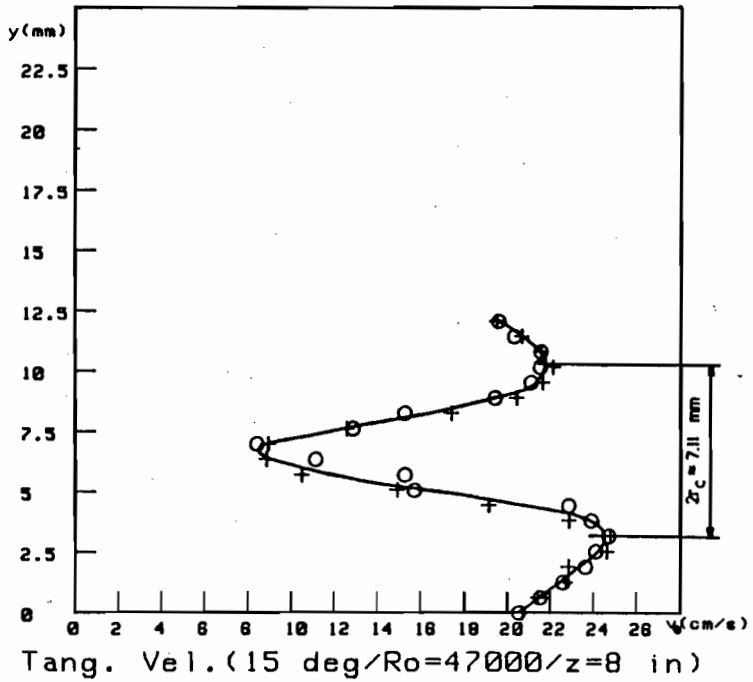

Fig. VII.6 Repeatability check of tangential velocity
(O = run 1; + = run 2) (MI)

VIII. Flow visualizations

To give a pictorial idea of the experimental flow conditions, two flow visualization photographs, Figs. VIII.1 and VIII.2, are presented. Figure VIII.1 shows surface flow streaklines obtained in a subsonic wind tunnel, for the foil pressure side. The technique used was to place rows of dots of a mixture of oil and titanium dioxide along the foil's span. These visualizations showed clearly flow separation and reattachment, and flow reversal zones.

Figure VIII.2 shows a flow visualization of the vortex in the water channel, obtained by injecting dye simultaneously through three holes near the tip of the foil. The roll-up process is clearly observed, although a great deal of information is lost when still pictures are used to document the flow. Certain peculiarities of this technique must be considered when interpreting the photographs. First of all, there is the question of whether the dye injection considerably affects the flow. This will depend on the

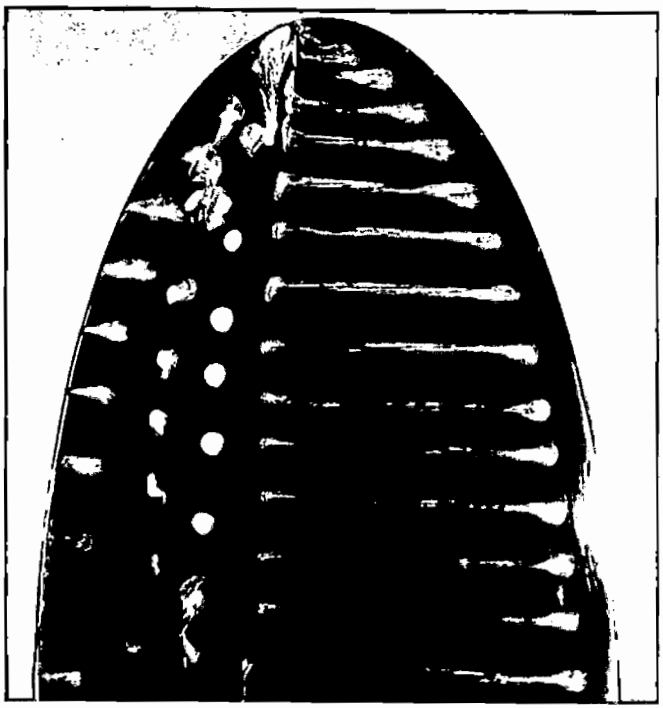

Fig. VIII.1 Pressure side surface flow streaklines ($R_0=2.7x10^5$, $\alpha=0^o$)

momentum of the dye upon its emergence from the injection hole. Ideally, the dye should emerge with negligible velocity from the hole, a condition which is difficult to establish. Secondly, there is the question of the speed at which the photographs are taken. Faster shutter speeds produce finer detail and eliminate blurring, but may provide a false impression of how the flow is developing. This is especially true for the roll-up process. In some photos, it appeared that vortex rings were issuing from each dye hole, with a tangential velocity component much greater than the axial velocity. Actually, this effect was due to the dye flowing in spurts from the holes. Sometimes the dye even subdivided itself into two or more filaments.

It is interesting to note in Fig. VIII.2 that the dye that locates itself in the vortex core comes not from the tip, but from a position on the trailing edge somewhat inward from the tip. This points once more to the comple-

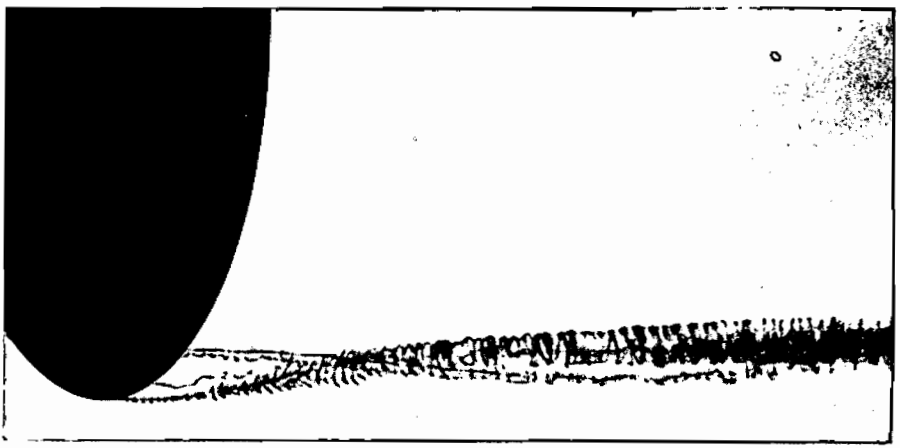

Fig. VIII.2 Visualization of tip vortex in water for $R_0 = 2.5 \times 10^4$ and $\alpha = 5°$. Dye injected from 3 holes on pressure side.

xity of these flows and the difficulties in both theoretical analyses and experimental studies.

IX. Concluding remarks

A review of the problem of tip-vortex roll-up for an elliptically-loaded wing has been presented, with particular reference to measurements recently carried out at the St. Anthony Falls Hydraulic Laboratory. The remarkable complexities of the flow phenomena involved pose challenges as yet not fully resolved for theoretical analyses and/or experimental investigations. The shortcomings and difficulties of available theories as examined in this review obviously require for their elucidation comprehensive experimental investigations. These, in turn, must take into account the three-dimensional nature of the flow and, as the analyses of experimental techniques for measurement of vortex core characteristics has shown, have difficulties and shortcomings of their own, which must be carefully considered in the planning of experiments.

A major factor to be considered in such planning is the asymmetry of the vortex core flow. Actually, the core structure appears to be strongly three-dimensional, and this may require not only a redefinition of what is meant by core radius but also a reexamination of available theoretical

models. The use of two-component (two-color) lasers with frequency shifting should help resolve some of the measurement difficulties discussed in preceding sections. However, the rather significant axial velocity reductions in the vortex core coupled with the possible strong three-dimensional core structure suggested by the present measurements, may require measurement of all three velocity components to elucidate some of the questions. In any event, the errors associated with the LDV measurements themselves (velocity biasing, bubble interference, precision of associated electronics), probe positioning errors, and errors due to vortex wandering, should be carefully evaluated in all cases. For vortices exhibiting strong unsteadiness, as is the case for example of intake vortices, the problems to be resolved for experimental measurement appear formidable indeed, and will require the use of sophisticated (and likely onerous) data acquisition schemes, whose development has been made possible by the technological advances in electronics and computer systems of the past decade.

NOMENCLATURE

a	distance between vortex cores.
	mean line pressure distribution of wing section
b	wing span
b′	distance between point vortices in Prandtl model
c	wing chord
c_l	section lift coefficient
c_{l_0}	midspan section lift coefficient
c_m	average chord
c_0	midspan chord
d	diameter of LDV focusing lens
$d_{e^{-2}}$	diameter of laser beam at crossing point
d_g	thickness of glass window
d_m	diameter of laser probe volume
f	focal length of LDV focusing lens
f′	focal length of LDV system after refraction
g	acceleration of gravity
h	height of free surface
h_c	h at center of vortex
h_m	height of laser probe volume
h_r	h at radius of vortex core
h_0	h at infinity
i	imaginary unit
$\vec{I}$	x-direction unit vector
$\vec{J}$	y-direction unit vector
k	slope of section lift curve, constant in Prandtl model
l	lens-to-window distance in LDV system
ℓ	characteristic length (McCormick)
l_m	length of laser probe volume
m_1	refractive index of air
m_2	refractive index of observation window (glass)
m_3	refractive index of test fluid (water)
n	constant exponent
p_c	vortex corepressure
p_r	pressure at edge of vortex core
p_v	vapor pressure
p_0	free-stream pressure
q	modulus of 2-D velocity vector
r	radial coordinate, empirical constant (McCormick)

r_c	vortex coreradius
r_1	specific radial coordinate in Betz model
t	time
u	x-component of velocity
v	y-component of velocity
$\vec{u}$	velocity vector
v_z	axial component of velocity
v_θ	tangential component of velocity
v_{45}	component of velocity at 45° to free stream
w	downwash velocity
w_a	average spanwise velocity (McCormick)
w_0	tangential velocity at edge of tip vortex (McCormick)
x	wing spanwise coordinate
x_c	abscissa of center of gravity of vorticity
x_0	abscissa of center of circle, station at edge of tip-vortex
x_1	specific spanwise coordinate in Betz model
y	coordinate perpendicular to wing planform
y_0	ordinate of center of circle
z	wing chordwise coordinate
AR	wing aspect ratio
C	contour of integration
Cp_{min}	minimum pressure coefficient
C_{Di}	wing induced drag coefficient
C_L	wing lift coefficient
C_1, C_2	arbitrary constants
$D_{e^{-2}}$	diameter of laser beam at exit from laser
Di	induced drag
E	LDV beam expander expansion ratio
K	constant
Kc	kinetic energy of vortex cores
Ki	total kinetic energy
Ko	kinetic energy of irrotational flow
L	lift
L_0	section lift per unit length at wing midspan
M1	LDV measurement technique in which tangential velocity is measured directly
M2	LDV measurement technique in which tangential velocity is obtained from the decomposition of two other components
R	Reynolds number
$\mathbf{R}_\ell$	Reynolds number based on characteristic length ℓ

R_0	Reynolds number based on midspan or root chord
S	area of wing, area of integration
U_0	free-stream velocity
V	reference velocity in McCormick's analysis
V_r	velocity along ℓ direction (McCormick)
Y	window-to-probe volume distance
Y′	window-to-probe volume distance after refraction
Z	complex variable
α	geometric angle of attack
α'	effective angle of attack ($\alpha - \alpha_0$)
α_0	angle of zero lift
γ	maximum circulation coefficient = $\Gamma_0/\sqrt{b}$ (Moore & Saffman)
ϵ	arbitrarily small number
θ	angular coordinate
κ_1	angle of incidence of laser beam on observation window
κ_2	angle of refracted laser beam in window
κ_3	half-angle of laser beam at probe volume
λ	compression factor (Moore & Saffman)
λ_3	wavelength of laser light in test fluid (water)
ν	kinematic viscosity
ξ	dimensionless spanwise coordinate (McCormick)
ρ	density
σ	cavitation number
σ_z	standard deviation of axial velocity component
σ_θ	standard deviation of tangential velocity component
σ_{45}	standard deviation of 45° velocity component
φ	angle between reference velocities (McCormick)
ω	complex potential
Γ	circulation
Γ_v	circulation of vortex
Γ_0	circulation at midspan chord
Δt	time interval
ϕ	velocity potential
ψ	stream function
ψ_c	value of stream function at vortex coreradius
Ω	angular velocity of vortex core

REFERENCES

1. ABBOTT, I.H., DOENHOFF, A.E. VON. *Theory of Wing Sections*. Dover Publications Inc., 1959.
2. ADRIAN, R.J., FINGERSON, L.M., *Laser Velocimetry, Theory, Application and Techniques*, Notes from LDV short course, Minneapolis, *MN*, July, 1984.
3. BAKER, G.R., BARKER, S.J., BOFAH, K.K., SAFFMAN, P.G., *Laser Anemometer Measurements of Trailing Vortices in Water*. J. Fluid Mechanics, Vol. 65, part 2, pp. 325-336, August, 1974.
4. BATCHELOR, G.K., *Introduction to Fluid Dynamics*, Cambridge University Press, 1967.
5. BETZ, A., *Behavior of Vortex Systems*, *NACA* TM-713, June, 1933, (translated from ZAMM, Bd. XII, Nr. 3, June, 1932).
6. DONALDSON, C. DUP., BILANIN, A.J., *Vortex Wakes of Conventional Aircraft*. AGARDograph No. 204, May, 1975.
7. DURAND, W. F., *Aerodynamic Theory* Vol. II, Div. E, Julius Springer, 1935.
8. DURST, F., MELLING, A., WHITELAW, J.H., *Principles and practice of Laser-Doppler anemometry*. Second Edition, Academic Press, 1981.
9. FARELL, C., CUOMO, A.R., *Introduction to the study of vortex dynamics and similitude in free surface flows*. Technical Report, Centro Tecnológico de Hidráulica, Departamento de Aguas e Energia Elétrica, São Paulo, Brazil, 1981.
10. Farell, C. Cuomo, A.R., CHARACTERISTICS AND MODELING OF INTAKE VORTICES: REVIEW AND ANALYSIS, Journal of Eng. Mechanics, Vol. 110, No. 5, May, 1984.
11. FRANCIS, M.S., *A wind tunnel investigation of the formation of trailing vortices*. Ph. D. Thesis, Univ. of Colorado at Boulder, 1976.
12. HOEIJMAKERS, H.W.M., VAATSTRA, W., *A higher order panel method applied to vortex sheet roll-up, AIAA* Journal, Vol 21, pp. 516-523, April, 1983.
13. JORDAN, P.F., *Structure of Betz vortex cores*, J. Aircraft, Vol. 10, No. 11, pp. 691-693, November, 1973.
14. KUIPER, G., *Cavitation inception on ship propeller models*, Ph. D. Thesis, Delft University, Rotterdam, Holland, 1981.
15. LA TORRE, R., *Study of tip vortex cavitation noise from foils*, Intl. shipbuilding Progress. Vol. 27, No. 307, pp. 66-85, March, 1980.
16. MANSOUR, N.N., *Numerical Simulation of the tip vortex off a low aspect ratio wing at transonic speed. AIAA* 22nd Aerospace Sciences Meeting, Reno, Nevada, 1984 (*AIAA*-84-0522).
17. MCCORMICK, B.W. JR., *On cavitation produced by a vortex trailing from a lifting surface*. J. of Basic Eng., No. 9, pp. 369-379, September, 1962.
18. MILNE-THOMSON, L.M., *Theoretical Aerodynamics*, Dover Publications Inc. 1958.
19. MISES, R. VON, *Theory of Flight*, Dover Publications Inc., 1959.
20. MOORE, D.W., SAFFMAN, P.G., *Axial flow in laminar trailing vortices* Proc. Royal Soc. London A333, pp. 491-508, 1973.

21. MOORE, D.W., *A numerical study of the roll-up of a finite vortex sheet,* J. Fluid Mechanics, 63, pt. 2, pp. 225-235, 1974.
22. PLATZER, G.P., SOUDERS, W.G., *Tip vortex cavitation delay with application to marine lifting surfaces, A literature survey,* Ship Performance Dept. Research and Development Report, David Taylor Naval Ship Research and Development Center, *DTNSRDC*-79/051, August, 1979.
23. QUADRELLI, J.C., *An experimental investigation of vortex roll-up for an eliptically-loaded wing,* M.S. Thesis, Univ. of Minnesota, 1985.
24. ROBERTSON, J.M., *Hydrodynamics in Theory and Application* Prentice-Hall, 1964.
25. RODAL, E.A.C., ALARCÓN, F.A.Z., GUEVARA, J.Y.G., GUEVARA, M.G.R., *Velocimetria Laser,* Undergraduate Thesis, Univ. of Mexico, Mexico City, 1983.
26. ROSSOW, V.J., *On the inviscid rolled-up structure of lift-generated vortices.* J. Aircraft, Vol. 10, No. 11, pp. 647-650, November, 1973.
27. SCHLICHTING, H., *Boundary Layer Theory* Seventh Edition, McGraw-Hill Book Co., 1979.
28. SOUDERS, W.G., PLATZER, G.P., *Tip vortex cavitation characteristics and delay of inception on a three-dimensional hydrofoil,* Ship performance Dept. Research and Development Report, David Taylor Naval Ship Research and Development Center, *DTNSRDC*-81/007, April, 1981.
29. SPREITER, J.R., SACKS, A.H., *The rolling up of the trailing vortex sheet and its effect on the downwash behind wings,* J. of the Aeronautical Sciences, Vol. 18, No. 1, pp, 21-32, January, 1951.
30. VERNON, D., *Analysis of a trailing tip vortex using laser Doppler velocimetry,* Senior Thesis in Aerospace Eng., Penn. State Univ., 1981.
31. WIDNALL, S.E., *The structure and dynamics of vortex filaments,* Annual Review of Fluid Mechanics, Vol. 7, 1975.